

# PriorDiffusion: Leverage Language Prior in Diffusion Models for Monocular Depth Estimation

Ziyao Zeng<sup>1</sup> Jingcheng Ni<sup>2</sup> Daniel Wang<sup>1</sup> Patrick Rim<sup>1</sup>  
 Younjoon Chung<sup>1</sup> Fengyu Yang<sup>1</sup> Byung-Woo Hong<sup>3</sup> Alex Wong<sup>1</sup>

<sup>1</sup>Yale University <sup>2</sup>Duke Kunshan University <sup>3</sup>Chung-Ang University<sup>3</sup>

<sup>1</sup>{ziyao.zeng, daniel.wang.dhw33, patrick.rim, fengyu.yang}@yale.edu

<sup>1</sup>{younjoon.chung, alex.wong}@yale.edu <sup>2</sup>jn189@duke.edu <sup>3</sup>hong@cau.ac.kr

## Abstract

Traditional monocular depth estimation suffers from inherent ambiguity and visual nuisance. We argue that language prior can enhance monocular depth estimation by leveraging the inductive bias learned during the text-to-image pre-training of diffusion models. The ability of these models to generate images that align with text indicates that they have learned the spatial relationships, size, and shape of specified objects, which can be applied to improve depth estimation. Thus, we propose PriorDiffusion, using a pre-trained text-to-image diffusion model that takes both images and corresponding text descriptions to infer affine-invariant depth through a denoising process. We also show that language prior enhances the model’s perception of specific regions of images that users care about and describe. Simultaneously, language prior acts as a constraint to accelerate the convergence of both training and the inference diffusion trajectory. By training on HyperSim and Virtual KITTI, we achieve faster training convergence, fewer inference diffusion steps, and state-of-the-art zero-shot performance across NYUv2, KITTI, ETH3D, and ScanNet. Code will be released upon acceptance.

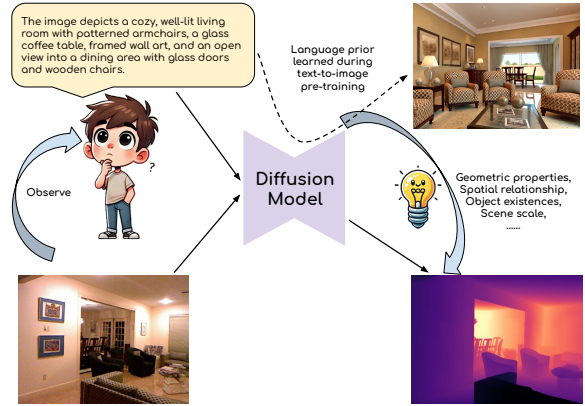


Figure 1. **Language prior in diffusion models enhances depth estimation** by leveraging the geometric prior aligned with the language description. It is learned during text-to-image generation pre-training, as to generate images under different viewpoints and layouts that accurately reflect the text, the model must comprehend the size and shape of specified objects, their spatial relationship, and the scale of the scene.

## 1. Introduction

Monocular depth estimation requires the model to predict pixel-wise depth from a single image. Recent advancements in diffusion-based models have shown promise for generating high-quality depth maps [11, 15, 17, 21, 24, 25, 29, 30, 57, 58, 65, 83] due to their ability to capture complex structures and fine details by progressively denoising a latent representation to produce accurate depth predictions. However, it remains a challenging task due to inherent ambiguities and various visual nuisances. Unlike stereo or multi-view depth estimation methods, monocular

approaches lack depth cues provided by multiple perspectives, leading to difficulty in accurately discerning the relative sizes, distances, and spatial relationships of objects within a scene. That is, different real-world 3D scenes can project to the same 2D image, causing inherent ambiguities. For example, texture ambiguity. Surfaces that are uniformly textured or have repetitive patterns, like tiled floors, can create confusion for depth estimators. The models might misinterpret the repetition as uniform depth, even though the actual depth might vary (e.g., a tiled floor receding into the distance). Also, visibility ambiguity creates limitations for discerning small, partial or occluded objects purely from the visual signal. On the other hand, visual nuisances such as illumination, motion blur, atmospheric conditions, and perspective distortion distort or obscure critical visual cues,

leading vision algorithms to misinterpret scene structure, depth, and object boundaries, thus reducing their accuracy and reliability.

Shown in Figure 1, an emerging solution lies in leveraging language as a complementary modality to provide a prior to resolve ambiguity and visual nuisance. Language descriptions provided by humans offer a wealth of priors about spatial relationships, scene types, object sizes, and depth hierarchies. In cases where an object is small, partially occluded, visually similar to the background, or its type is ambiguous from a single image, language can indicate the object’s identity and semantics, enabling the model to infer its typical 3D size and shape and make more precise depth predictions for the observed portion. Language inputs are also valuable in resolving texture ambiguities. Descriptive cues can specify the type and function of surfaces in a scene, aiding the model in inferring geometric properties. For instance, if a uniformly textured surface is described as a “white ceiling”, the model can interpret it as a continuous, flat plane at a consistent depth above the observer, extending into the distance. Similarly, for surfaces with repetitive patterns, such as a red and black interwoven carpet, language inputs like “A red and black interwoven carpet extending across the room” can help the model recognize that the repeating pattern belongs to a flat surface, preventing misinterpretation of edges between tiles as depth discontinuities. As shown in Figure 2, better perception can be achieved for insignificant regions indicated in the language description.

To this end, we propose PriorDiffusion, incorporating human-provided language prior of the scene as an inductive bias to guide the depth map prediction. During text-to-image pre-training, diffusion models learn to generate diverse images under various viewpoints and scene layouts that align with the provided language descriptions. The ability of these models to generate images that align with text suggests they have learned the spatial relationships, size, and shape of specified objects in the described 3D scene, which can be leveraged to improve depth estimation. In our PriorDiffusion, during the denoising process, both the image and the text input are used by the model as conditions to predict the noise to be removed. Ultimately, Gaussian noise is progressively refined into a depth map that aligns with both the input image and the language description. In real-world applications when embodied agents are integrated with PriorDiffusion, humans can describe the environment to help agents better perceive it. When generalizing to a new environment, language, having less covariate shift compared to images, allows humans to describe the new environment, aiding agents in better adapting and generalizing to it.

To support our hypothesis, we conduct training on two synthetic datasets, HyperSim [53] and Virtual KITTI [3], and conduct zero-shot evaluation on four real-world



Figure 2. **3D reconstruction.** For insignificant regions indicated in language description, PriorDiffusion achieves better depth estimates and reconstructions thanks to the use of language.

datasets, NYUv2 [60], KITTI [22], ETH3D [59], and ScanNet [9]. Given the difficulty of obtaining sufficient human-provided text descriptions for every training and inference image, we utilize a vision-language model, i.e. LLaVA [10], to generate descriptions for each image, simulating human annotation. we achieve faster training convergence, fewer inference diffusion steps, and state-of-the-art zero-shot performance across NYUv2, KITTI, ETH3D, and ScanNet.

**Our contributions.** By leveraging language prior for diffusion-based monocular depth estimation, we demonstrate that:

- Language prior provides an inductive bias about the existence, geometric properties, and spatial relationships of objects specified in the language description, allowing depth estimators to better perceive the depth of those objects.
- Language prior directs the model’s attention to specific regions, guiding it to perceive the 3D scene according to the user’s intent. This is particularly beneficial for regions that pose challenges to vision systems, such as those with small size, poor illumination, occlusion, or high visual similarity to the background.
- Language prior serves as a constraint to speed up training convergence, and serves as a good initialization of diffusion trajectory to speed up inference. This improves the efficiency of the diffusion model, optimizing both its performance and computational resource usage.

## 2. Related Work

**Monocular depth estimation.** Monocular depth estimation is a dense regression problem, requiring pixel-wise predictions of depth from a single image, capturing complex spatial relationships within the scene. Some depth models learn to infer pixel-wise depth in metric scale (i.e. meters) [2, 16, 32, 39, 64, 73, 74, 81] by minimizing loss between depth predictions and ground-truth depth maps. Each

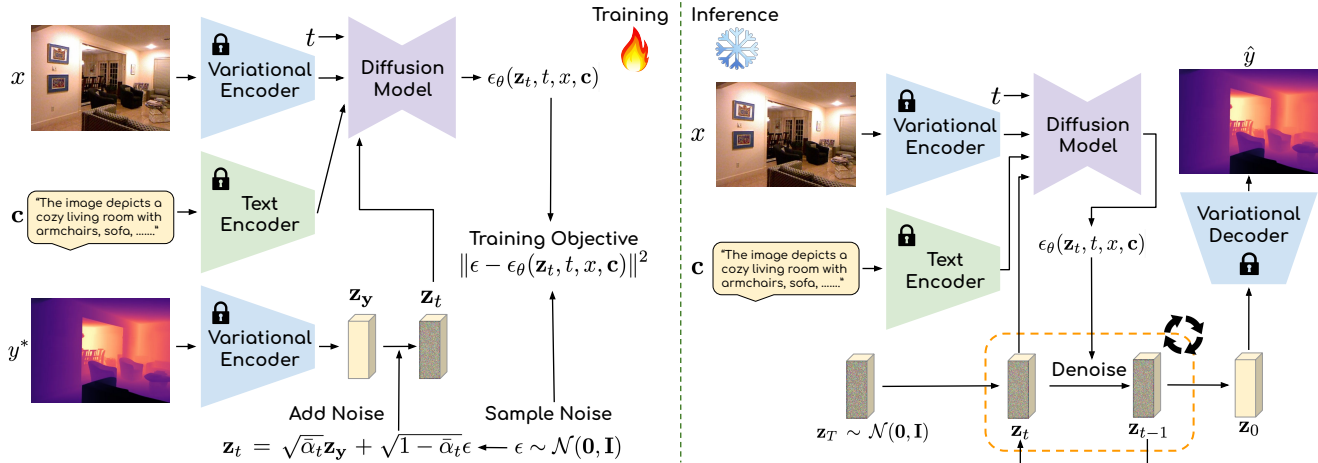


Figure 3. **Pipeline of PriorDiffusion.** We train the diffusion model to predict the noise added into the noisy depth latent  $\mathbf{z}_t$  at the time step  $t$ , based on  $\mathbf{z}_t$ , the input image  $x$ , and the corresponding language description  $c$ . During inference, the diffusion model predicts noise for  $\mathbf{z}_t$  at each time step and gradually denoise it from  $\mathbf{z}_T$  (pure Gaussian noise) into  $\mathbf{z}_0$  (pure depth latent). Then  $\mathbf{z}_0$  is decoded into the depth prediction using a frozen variational decoder.

model typically applies to only one data domain in which it is trained, with similar camera parameters and object scales. To enable generalization across diverse domains, empowering depth estimation in the wild, other works have explored affine-invariant depth estimation [12, 30, 38, 50, 51, 68, 69, 71, 72, 76], which predicts depth up to an unknown global shift and scale. This approach can accommodate varied scenes with different scales, while still preserving the geometric relationships between different objects or regions within the scene. HND [76] hierarchically normalizes the depth representations with spatial information and depth distributions. Depth Anything [68] learns from large-scale automatically annotated data. DPT [51] leverages vision transformers using a scale- and shift-invariant trimmed loss. MiDAS [50] mixes multiple datasets with training objectives invariant to depth range and scale. Depth Anything [68] and Depth Anything v2 [69] train a depth foundation model using large-scale unlabeled data. Existing methods try to predict depth solely from images, which suffers from ambiguity like scale, object orientation, occlusion, and visual nuisance like viewpoints, illumination, appearance, texture, etc. On the other hand, our PriorDiffusion leverages language prior in Diffusion Models to provide a thorough understanding of the scene associated with the input text, to resolve the ambiguity and the nuisance variables in the visual algorithm.

**Diffusion model for monocular depth estimation.** Denoising Diffusion Probabilistic Model (DDPM) [26] learns to reverse a diffusion process that progressively degrades images with Gaussian noise so that they can draw samples from the data distribution by applying the reverse process to random noise. They have been applied to various tasks like text-to-image generation [49, 54, 63, 88, 89], super res-

olution [20, 35, 55], image inpainting [8, 42, 70], 3D object generation [34, 41, 46], etc. Several approaches have explored the use of DDPM for metric depth estimation. DiffusionDepth [11] learns to denoise random depth distribution into a depth map with monocular visual conditions. Similarly, DDP [29] encodes the input image and use diffusion to decodes it into a depth map. DepthGen [57] extends a multi-task diffusion model for metric depth prediction. Its successor, DDVM [58], focuses on pretraining with synthetic and real datasets to improve depth estimation performance. Build upon the diffusion model, DepthFM [24] uses flow matching to conduct a faster monocular depth estimation. In light of strong representation learned by pre-trained, text-to-image diffusion models, recent methods like VPD [83], E2E FT [21], GeoWizard [17], Lotus [25], GenPercept [65], and Marigold [30] utilize a pretrained Stable Diffusion model [54] as a backbone to predict depth through a denoising process. Specifically, Marigold [30] concatenates input images with diffusion latent as conditions for denoising U-Net to predict noise that needs to be removed, to gradually denoise a Gaussian noise to a depth map. While previous works only focused on using images as conditions of diffusion models to predict depth, our PriorDiffusion utilizes language prior as inductive bias for diffusion models to resolve ambiguity and visual nuisances, and conduct 3D perception in a controllable way.

**Language for monocular depth estimation.** Vision-Language models [4, 36, 37, 45, 48] acquire a comprehensive understanding of languages and images through pre-training under diverse datasets, thereby establishing a robust foundation for downstream tasks. [6, 31, 43, 62, 66, 67, 74, 75, 79–81, 87]. For example, CLIP [48] use contrastive learning on text-image pairs, which allows for

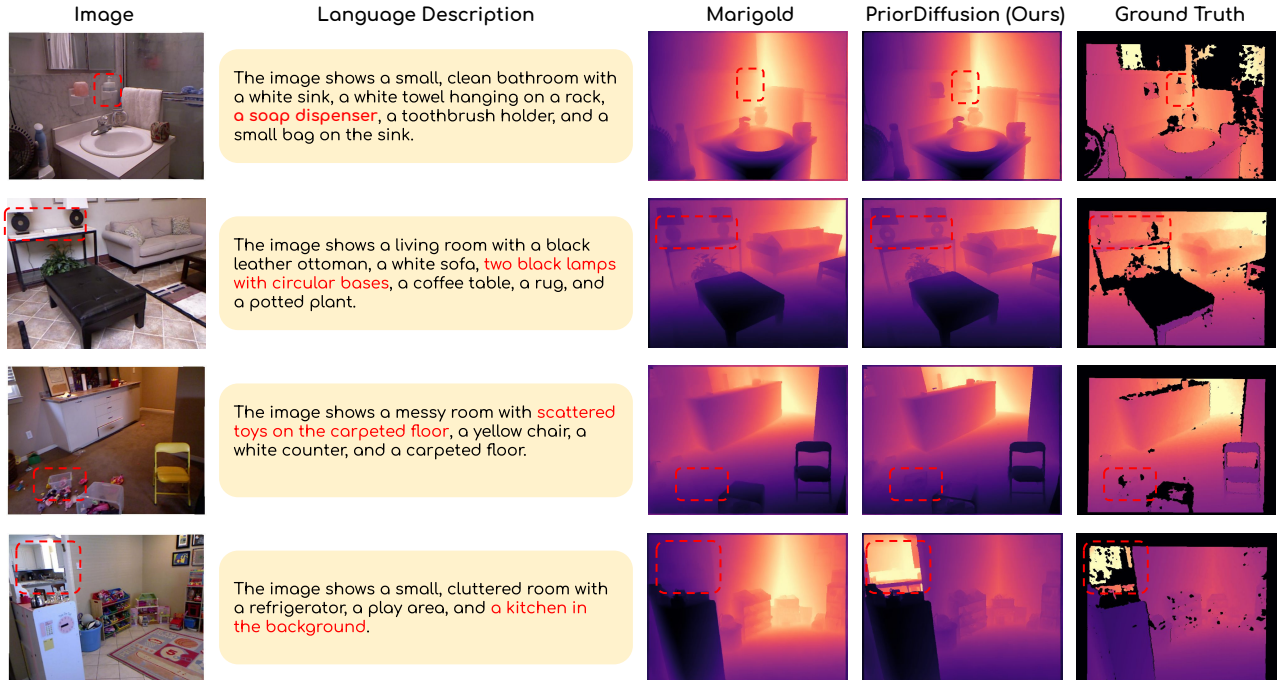


Figure 4. **Visualization on NYUv2.** Compared to Margold, our PriorDiffusion demonstrates more accurate depth prediction for a given input image, particularly for instances specified in the language description (marked in red). This is achieved by leveraging the language prior within the text-to-image diffusion model, enhancing the model’s ability to comprehend the geometric characteristics of these objects. Additionally, the language description directs the model’s attention to relevant regions, especially the ones that are easily neglected by visual signals, like “a soap dispenser” in the first row. It enables the depth estimator to perceive the 3D scene in a more controlled manner that aligns with the user’s interest.

various applications. These include few-shot image classification [19, 47, 78], object detection [52, 86], image segmentation [52, 84], and 3D perception [7, 28, 77, 80, 81, 85, 87]. Given their growing capabilities, some research [1, 28, 81, 82] has focused on applying vision-language models to monocular depth estimation. Specifically, DepthCLIP [81] utilizes CLIP’s semantic depth response as an ordinal relationship alongside a depth projection method to conduct zero-shot monocular depth estimation. WorDepth [74] learns the variational prior distribution of 3D scenes from text. RSA [75] predicts scale using language description to align relative depth to metric scale. While language has been applied in various aspects of 3D perception, our work is the first to use language prior for diffusion models to enhance 3D perception.

### 3. Method

**Problem formulation.** Formally, given an RGB image  $x : \Omega \subset \mathbb{R}^2 \rightarrow \mathbb{R}^3$ , the objective of monocular depth estimation is to predict a dense depth map  $y : \Omega \subset \mathbb{R}^2 \rightarrow \mathbb{R}_+$  using a parameterized function  $h$ , typically represented as a neural network, such that  $y := h(x)$ . We employ a supervised dataset  $\mathcal{D} = \{x^{(m)}, \mathbf{c}^{(m)}, y^{*(m)}\}_{m=1}^M$  comprised

of  $M$  samples, where  $y^* : \Omega \subset \mathbb{R}^2 \rightarrow \mathbb{R}_+$  denotes the ground-truth depth map, and  $\mathbf{c}$  signifies the corresponding text caption of the image.

**Diffusion formulation.** The pipeline of PriorDiffusion is shown in Figure 3. To use a diffusion model for monocular depth estimation, following the formulation of [11, 29, 30, 57, 58, 83], we adopt the formulation of Denoising Diffusion Probabilistic Model (DDPM) [26] for the forward diffusion process, reverse diffusion process, training objective and inference mentioned below. A latent variable  $\mathbf{z}_t \in \mathbb{R}^{H' \times W' \times C'}$  is defined to represent a noisy version of the depth map in the latent space at diffusion timestep  $t$ . The ground truth depth map  $y^*$  is encoded into a latent representation  $\mathbf{z}_y$  as supervision using a frozen VAE encoder  $E$ :  $\mathbf{z}_y = E(y^*)$ . The diffusion latent after the whole denoising process  $\mathbf{z}_0$  is decoded back to the image space using the frozen VAE decoder  $D$ :  $\hat{y} = D(\mathbf{z}_0)$ .

**Forward diffusion process.** The forward process gradually adds noise to the latent depth feature in  $T$  steps. The process can be defined as:

$$q(\mathbf{z}_t | \mathbf{z}_{t-1}) = \mathcal{N}(\mathbf{z}_t; \sqrt{1 - \beta_t} \mathbf{z}_{t-1}, \beta_t \mathbf{I}),$$

where  $\beta_t$  is a scalar that defines the variance of the Gaussian noise added at each step  $t$  in the forward diffusion process.

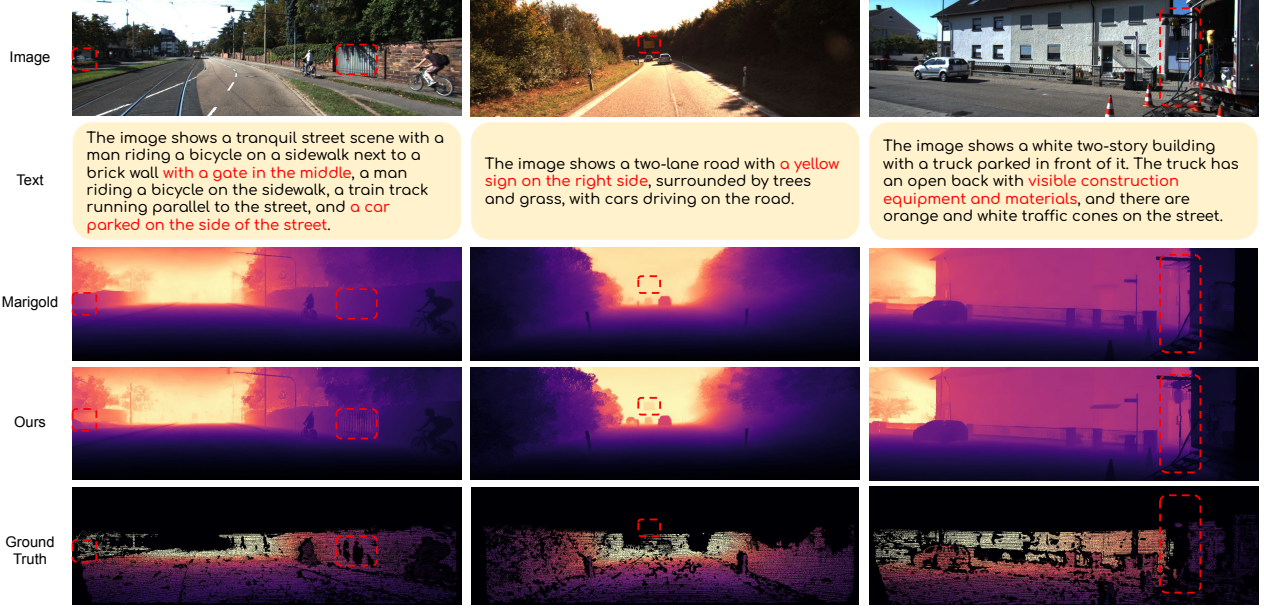


Figure 5. **Visualization on KITTI.** PriorDiffusion predicts better depth for described objects, even when parts of the object are almost visible in the image (such as the parking car in the first column). The model is guided for specific described regions, such as a sign at a distance, potentially enhancing the safety of self-driving systems that rely solely on vision sensors.

This parameter controls how much noise is added into the latent variable  $\mathbf{z}_t$  as it transitions from  $\mathbf{z}_{t-1}$  over time.

The forward process from  $y$  to  $\mathbf{z}_T$  can be written as:

$$q(\mathbf{z}_{1:T}|y^*) = \prod_{t=1}^T q(\mathbf{z}_t|\mathbf{z}_{t-1}),$$

where  $D(\mathbf{z}_0) = \hat{y}$ .

**Reverse diffusion process.** The goal of the reverse process is to denoise  $\mathbf{z}_T$  to recover  $\hat{y}$ . The reverse process is defined as:

$$p_\theta(\mathbf{z}_{0:T}|x, \mathbf{c}) = p(\mathbf{z}_T) \prod_{t=1}^T p_\theta(\mathbf{z}_{t-1}|\mathbf{z}_t, x, \mathbf{c}),$$

where  $p(\mathbf{z}_T)$  is assumed to be a standard Gaussian distribution  $\mathcal{N}(\mathbf{z}_T; \mathbf{0}, \mathbf{I})$ , and the denoising step  $p_\theta(\mathbf{z}_{t-1}|\mathbf{z}_t, x, \mathbf{c})$  is parameterized as:

$$p_\theta(\mathbf{z}_{t-1}|\mathbf{z}_t) = \mathcal{N}(\mathbf{z}_{t-1}; \mu_\theta(\mathbf{z}_t, t, x, \mathbf{c}), \Sigma_\theta(\mathbf{z}_t, t, x, \mathbf{c})),$$

where  $\mu_\theta$  and  $\Sigma_\theta$  is the diffusion model, that predicts the mean and variance conditioned on  $\mathbf{z}_t$ ,  $t$ , the input image  $x$  and the corresponding text  $\mathbf{c}$ . We use the denoising U-Net from Stable Diffusion v2 [54] to initialize is the diffusion model. Specifically, given a text caption  $\mathbf{c} = \{c_1, c_2, \dots\}$ , we first encode it through a frozen CLIP text encoder, then feed it into the diffusion model. Given an image  $x$ , we encode it using the same VAE encoder  $E(x)$  that encoded the

depth map, concatenated with the depth latent  $\mathbf{z}_t$ , then feed it into the diffusion model.

**Training objective.** Our training objective is derived using the reparameterization trick and variational bounds, which involves predicting the noise added at each step. The loss function is:

$$\mathcal{L}(\theta) = \mathbb{E}_{y, \epsilon, t} [\|\epsilon - \epsilon_\theta(\mathbf{z}_t, t, x, \mathbf{c})\|^2],$$

where:  $\epsilon \sim \mathcal{N}(\mathbf{0}, \mathbf{I})$  is the noise sampled during the forward process, and  $\mathbf{z}_t = \sqrt{\bar{\alpha}_t} \mathbf{z}_y + \sqrt{1 - \bar{\alpha}_t} \epsilon$  is the noisy depth map at step  $t$ , where  $\bar{\alpha}_t = \prod_{s=1}^t (1 - \beta_s)$ .

**Inference.** The inference phase begins by sampling a purely noisy latent variable  $\mathbf{z}_T$  from a standard Gaussian distribution,  $\mathbf{z}_T \sim \mathcal{N}(\mathbf{0}, \mathbf{I})$ . This initial noisy sample represents the starting point of the reverse diffusion process. The goal is to progressively refine this sample through a series of denoising steps until the final depth latent  $\mathbf{z}_0$  is obtained. Each denoising step is to predict the noise component  $\epsilon_\theta(\mathbf{z}_t, t, x, \mathbf{c})$  that needs to be removed from the latent variable at time step  $t$ . The prediction is made by the diffusion model conditioned on the noisy latent  $\mathbf{z}_t$ , the current timestep  $t$ , the input image  $x$ , and the corresponding text description  $\mathbf{c}$ . The iterative denoising process follows the reverse transition:

$$\mathbf{z}_{t-1} = \frac{1}{\sqrt{\alpha_t}} \left( \mathbf{z}_t - \frac{1 - \alpha_t}{\sqrt{1 - \bar{\alpha}_t}} \epsilon_\theta(\mathbf{z}_t, t, x, \mathbf{c}) \right),$$

where  $\alpha_t$  and  $\bar{\alpha}_t$  are derived from the noise schedule  $\beta_t$ . This reverse diffusion continues until  $t = 0$ , at which point

Method	Training Images	NYUv2		KITTI		ETH3D		ScanNet	
		$\delta_1 \uparrow$	AbsRel $\downarrow$						
<i>Methods using more than 100K training images</i>									
GeoWizard [17]	280K	96.3	5.6	82.0	14.4	<b>95.8</b>	<b>6.6</b>	95.0	6.4
HDN [76]	300K	94.8	6.9	86.7	11.5	83.3	12.1	93.9	8.0
DiverseDepth [71]	320K	87.5	11.7	70.4	19.0	69.4	22.8	88.2	10.9
LeReS [72]	354K	91.6	9.0	78.4	14.9	77.7	17.1	91.7	9.1
DPT [51]	1.4M	90.3	9.8	90.1	10.0	94.6	7.8	93.4	8.2
MiDaS [50]	1.9M	88.5	11.1	63.0	23.6	75.2	18.4	84.6	12.1
Omnidata [12]	12.2M	94.5	7.4	83.5	14.9	77.8	16.6	93.6	7.5
Depth Anything v2 [69]	62.6M	97.9	4.4	<b>94.8</b>	<b>7.5</b>	86.2	13.2	97.8	<b>4.2</b>
Depth Anything [68]	63.5M	<b>98.1</b>	<b>4.3</b>	94.7	7.6	88.2	12.7	<b>98.1</b>	4.3
<i>Methods using less than 100K training images</i>									
Marigold [30]	74K	95.9	6.0	90.4	10.5	95.1	7.1	94.5	6.9
Marigold* (iter: 20000)	74K	95.2	6.4	86.2	12.0	93.9	7.6	94.8	7.1
Marigold* (iter: 30000)	74K	95.7	6.1	89.7	10.7	95.4	6.9	94.0	7.3
<b>PriorDiffusion (Ours)</b> (iter: 20000)	74K	95.9	6.0	<b>90.6</b>	<b>10.4</b>	95.6	6.6	94.4	7.1
<b>PriorDiffusion (Ours)</b> (iter: 30000)	74K	<b>96.0</b>	<b>5.9</b>	90.3	<b>10.4</b>	<b>95.8</b>	<b>6.5</b>	<b>94.9</b>	<b>6.7</b>

Table 1. **Quantitative comparison.** PriorDiffusion achieves performance on par with other state-of-the-art affine-invariant depth estimators that use significantly more training images, and outperforms methods trained with a similar number of images. Metrics are reported as percentages. \* indicates the results of the model that we re-implemented. Note that our method converges faster compared with Marigold, and is even better with only two-thirds iterations, attributing the language prior which provides a stronger constraint for the fast convergence of the diffusion trajectory. For fair comparison, PriorDiffusion and Marigold are evaluated without ensemble.

the fully denoised latent  $\mathbf{z}_0$  is reached. The predicted depth map  $\hat{y}$  is obtained by decoding  $\mathbf{z}_0$  back into the image space using the pre-trained and frozen VAE decoder:  $\hat{y} = D(\mathbf{z}_0)$ .

## 4. Experiments

**Training datasets.** We adopt the training scheme of Marigold [30], and train our PriorDiffusion on two synthetic datasets that cover both indoor and outdoor scenes. The first dataset utilized is HyperSim [53], a photorealistic compilation of 461 indoor scenes. From HyperSim, approximately 54,000 samples is selected from 365 scenes, adhering to the official data split and excluding any incomplete samples. RGB images and their corresponding depth maps are resized to a resolution of  $480 \times 640$  pixels. The second dataset is Virtual KITTI [3, 18], which comprises synthetic street scenes across five distinct settings, with varied conditions such as different weather patterns and camera perspectives. We specifically use the Virtual KITTI 2 [3] version. For training, we select four scenes, totaling approximately 20,000 samples.

**Depth normalization for training.** Following [30, 50, 51, 68], to standardize the ground truth depth maps  $\mathbf{d}$ , we apply a linear normalization ensuring that the depth values primarily fall within the range  $[-1, 1]$ , aligning with the input value range of the VAE. It ensures an affine-invariant depth representation that remains robust to data statistics, guaranteeing that all scenes are constrained by near and far planes with extreme depth values. The affine transformation for

normalization is defined as:

$$\tilde{y}^* = \left( \frac{y^* - y_2}{y_{98} - y_2} - 0.5 \right) \times 2, \quad (1)$$

where  $y_2$  and  $y_{98}$  represent the 2% and 98% percentiles of the depth maps, respectively.

**Evaluation datasets.** We assess the performance of our PriorDiffusion using 4 real-world datasets that were not part of its training data, following the configuration as Marigold [30]. Both NYUv2 [60] and ScanNet [9] consist of indoor scenes captured with an RGB-D Kinect sensor. For NYUv2, we use the specified test set, containing 654 images. With ScanNet, we randomly select 800 images from the 312 official validation scenes for evaluation. The KITTI dataset [22, 23] features outdoor street scenes with sparse metric depth captured by a LiDAR sensor, where we apply the Eigen test split [13] consisting of 652 images, following the evaluation protocol of [14]. For ETH3D [59], which are also based on LiDAR measurements, we use all 454 samples that include ground truth depth maps. Following the affine-invariant depth evaluation protocol [30, 50, 51, 68, 75], we evaluate first-order threshold accuracy  $\delta_1$  and mean absolute relative error *AbsRel*. Details of the metric are provided in the supplementary material.

**Obtain language description.** To implement our method, we require human-provided text descriptions for each image. Since standard benchmarks do not include such descriptions, we propose using off-the-shelf models to generate text descriptions to simulate those a human would

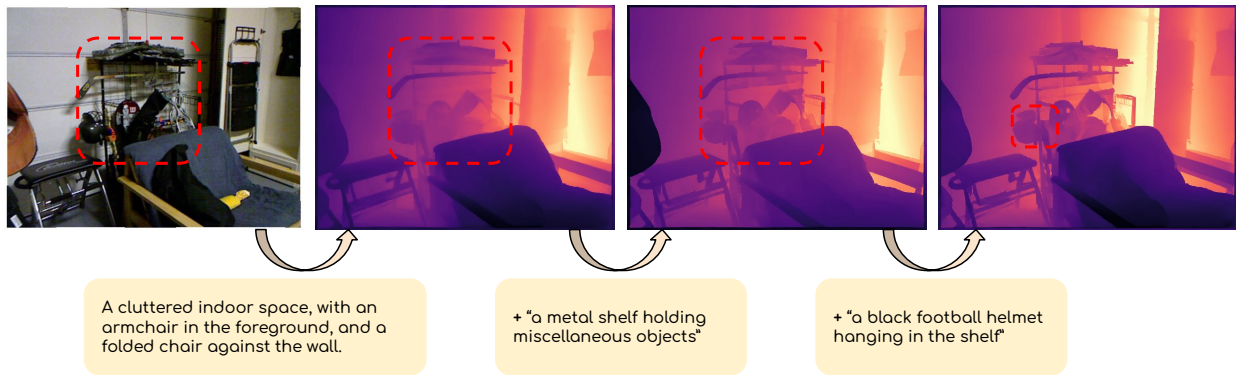


Figure 6. **Controllable depth estimation with language.** Each time, we append the newly added sentence to the end of the original sentence and repeat the inference process. It shows that by providing more details in the language, our method predicts more accurate depth for those specified regions or objects.

provide. For this purpose, we use the visual question-answering model LLaVA v1.6 [40] to generate 10 text descriptions for each training image using different prompts, and 1 text description for each testing image for evaluation. The details of prompt design are shown in the supplementary material. In each training step, we randomly select 1 text out of 10 that aligns with the input image.

**Implementation details.** We follow the setup of Marigold [30]. Our method is implemented using PyTorch, using Stable Diffusion v2 [54] as the backbone model. During training, we use the DDPM noise scheduler [26] with 1000 diffusion steps. For inference, we use the DDIM scheduler [61] with 50 sampling steps. Our training process spans 30,000 iterations, with an effective batch size of 32 achieved through gradient accumulation over 16 steps (each with a per-step batch size of 2) to facilitate single-GPU execution. Optimization is performed using the Adam optimizer with a learning rate of  $3 \cdot 10^{-5}$ . Additionally, random horizontal flipping is applied as a data augmentation. Training to convergence, which typically occurs after 20,000 iterations for our method, required approximately four days on an Nvidia RTX 3090 GPU.

**Quantitative comparison.** Shown in Table 1, PriorDiffusion matches the performance of state-of-the-art affine-invariant depth estimators that require significantly more training images, while outperforming methods trained with a similar number of images. Another significant advantage of PriorDiffusion is its faster convergence. Compared to Marigold, even at 20,000 iterations, PriorDiffusion achieves performance metrics comparable to or better than Marigold’s results at 30,000 iterations. This is also demonstrated in Figure 7. This can be attributed to the language prior integrated into our model, which provides additional semantic and geometric prior serving as an extra constraint that speeds up diffusion training. An intuitive explanation is that the model expends less effort in learning the geo-

metric properties and spatial relationships of objects from the image, which is high-dimensional and computationally intensive to process. Instead, much of these features are already embedded in the language input, where these features are represented in a condensed and low-dimensional format, which is easier to learn.

**Qualitative comparison.** Besides the overall quantitative improvement, we claim that language prior can also guide the model’s attention to better perceive the region that is specified in the language description, which aligns more with users’ interests. The visualization for NYUv2 [60] is shown in Figure 4, where our PriorDiffusion achieves more accurate depth prediction for a given input image compared to Marigold, especially for instances highlighted in the language description. For instance, in the first row, the soap dispenser is barely distinguishable in the input image due to its color and texture blending with the background. Vision-based depth estimators like Marigold struggle to identify it, resulting in a depth prediction that matches the background. In contrast, the language description explicitly includes the term “a soap dispenser”, providing the model with a geometric and spatial prior that indicates the existence of a soap dispenser and what it should look like. Consequently, our PriorDiffusion can more accurately perceive the depth of the soap dispenser. Similarly, as shown in Figure 5, we visualize results for the KITTI [22] dataset, where objects such as a parked car or a sign are barely discernible from the visual signal alone. As shown in Figure 6, by incorporating more detailed language descriptions, depth predictions are enhanced for the specified regions or objects.

**Faster training convergence.** One of the key advantages of PriorDiffusion is its faster convergence compared to Marigold. As shown in Figure 7 here, the improved convergence can be attributed to the integration of a language prior in our model, which provides additional semantic and geometric constraints that help accelerate the diffusion process.

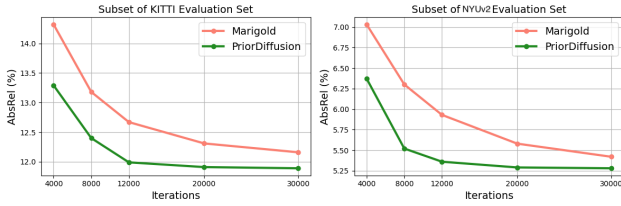


Figure 7. **Convergence speed comparison.** PriorDiffusion converges faster during training compared with Marigold, since it’s more efficient to learn 3D property from condensed, low-dimensional language feature.

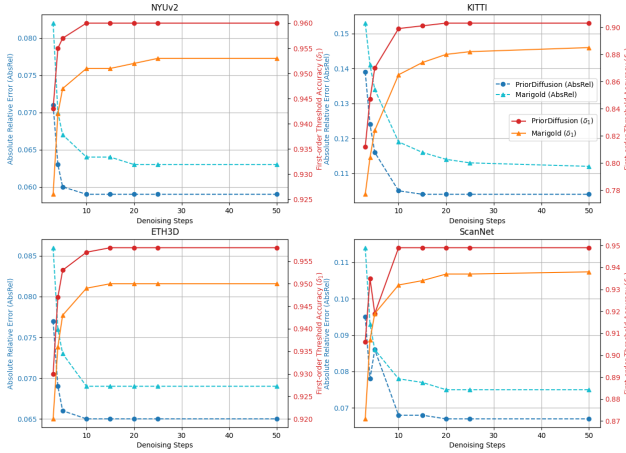


Figure 8. **Performance under different denoising steps.** PriorDiffusion consistently outperforms Marigold across various denoising steps, with a faster convergence.

Due to computation overhead, following the same configuration of Marigold, we use a subset of KITTI and NYUv2 for training-time evaluation.

**Fewer denoising steps.** As demonstrated in Figure 8, and detailed in Table 4 in the supplementary material, we evaluate PriorDiffusion and Marigold with different denoising steps during inference. PriorDiffusion consistently outperforms Marigold across different denoising steps. Remarkably, PriorDiffusion converges in just 10 steps, while Marigold takes 25 steps to achieve convergence. This indicates that the language prior serves as an effective initialization of the diffusion trajectory, enabling faster convergence.

**Better perception in small areas.** To demonstrate a better perception for small objects and areas mentioned in text, as shown in Figure 4. We use MaskDINO to obtain panoptic segmentation masks for all images in NYUv2 test set, then evaluate the performance for masks that occupied less than 5%, 10%, and 20% of an image. Table 2 shows that small areas are harder to perceive compared with large areas, and PriorDiffusion obtains better improvement over small areas, as language prior provides geometric and semantic properties that guide the diffusion model to better perceive small areas and tiny structures.

NYUv2	Standard		Small Area (5%)		Small Area (10%)		Small Area (20%)	
	$\delta_1 \uparrow$	AbsRel $\downarrow$						
Marigold	95.7	6.1	91.7	9.0	92.2	8.4	93.9	7.3
Ours	<b>95.9</b>	<b>5.9</b>	<b>92.8</b>	<b>8.3</b>	<b>93.1</b>	<b>7.9</b>	<b>94.6</b>	<b>6.8</b>

Table 2. **Better perception in small areas.** We evaluate the performance for panoptic segmentation masks that occupied less than 5%, 10%, and 20% of an image. PriorDiffusion obtains better improvement over small areas due to geometric properties of those areas offered by the language prior.



Figure 9. **Failure cases.** Incorrect text (here we replace ”a bookshelf with glass” with ”a window with curtains”) misguides PriorDiffusion to perceive the geometry of objects.

## 5. Discussion

**Conclusion.** We present PriorDiffusion, a novel approach that integrates language prior with diffusion models to enhance monocular depth estimation. By leveraging geometric prior learned by text-to-image model that associates with language, PriorDiffusion overcomes traditional ambiguities and visual nuisances associated with monocular depth estimation, achieving state-of-the-art performance across various zero-shot benchmarks, while maintaining a faster convergence for training and inference diffusion trajectory.

**Limitation.** One primary limitation is its dependence on the accuracy and detail of the provided language descriptions. Shown in Figure 9, ambiguous or misleading text inputs from human users can result in suboptimal depth predictions and potentially compromise the model’s performance. Last, our method requires language input from users, which may not always be feasible. In cases where user-provided descriptions are unavailable, as demonstrated in Figure 5 in the supplementary material, our method can still function with standardized template prompts. Another potential solution is to generate language descriptions on the fly using a vision-language model [10], an image captioner [27], or by following methods like RSA [75] to create structured text from the output of visual algorithm [33, 86]. While we have not explored this approach in this paper, it presents a promising avenue for future research.

## References

[1] Dylan Auty and Krystian Mikolajczyk. Learning to prompt clip for monocular depth estimation: Exploring the limits of human language. In *Proceedings of the IEEE/CVF International Conference on Computer Vision*, pages 2039–2047, 2023. 4

- [2] Shariq Farooq Bhat, Ibraheem Alhashim, and Peter Wonka. Adabins: Depth estimation using adaptive bins. In Proceedings of the IEEE/CVF Conference on Computer Vision and Pattern Recognition, pages 4009–4018, 2021. [2](#), [1](#)
- [3] Johann Cabon, Naila Murray, and Martin Humenberger. Virtual kitti 2. arXiv preprint arXiv:2001.10773, 2020. [2](#), [6](#), [1](#)
- [4] Mathilde Caron, Hugo Touvron, Ishan Misra, Hervé Jégou, Julien Mairal, Piotr Bojanowski, and Armand Joulin. Emerging properties in self-supervised vision transformers. In Proceedings of the IEEE/CVF international conference on computer vision, pages 9650–9660, 2021. [3](#)
- [5] Wenjie Chang, Yueyi Zhang, and Zhiwei Xiong. Transformer-based monocular depth estimation with attention supervision. In 32nd British Machine Vision Conference (BMVC 2021), 2021. [2](#)
- [6] Jiaben Chen, Renrui Zhang, Dongze Lian, Jiaqi Yang, Ziyao Zeng, and Jianbo Shi. iquery: Instruments as queries for audio-visual sound separation. In Proceedings of the IEEE/CVF Conference on Computer Vision and Pattern Recognition, pages 14675–14686, 2023. [3](#)
- [7] Runnan Chen, Youquan Liu, Lingdong Kong, Xinge Zhu, Yuexin Ma, Yikang Li, Yuenan Hou, Yu Qiao, and Wenping Wang. Clip2scene: Towards label-efficient 3d scene understanding by clip. In Proceedings of the IEEE/CVF Conference on Computer Vision and Pattern Recognition, pages 7020–7030, 2023. [4](#)
- [8] Ciprian Corneanu, Raghudeep Gadde, and Aleix M Martinez. Latentpaint: Image inpainting in latent space with diffusion models. In Proceedings of the IEEE/CVF Winter Conference on Applications of Computer Vision, pages 4334–4343, 2024. [3](#)
- [9] Angela Dai, Angel X Chang, Manolis Savva, Maciej Habber, Thomas Funkhouser, and Matthias Nießner. Scannet: Richly-annotated 3d reconstructions of indoor scenes. In Proceedings of the IEEE conference on computer vision and pattern recognition, pages 5828–5839, 2017. [2](#), [6](#), [1](#)
- [10] Zhicheng Ding, Panfeng Li, Qikai Yang, and Siyang Li. Enhance image-to-image generation with llava-generated prompts. In 2024 5th International Conference on Information Science, Parallel and Distributed Systems (ISPDS), pages 77–81. IEEE, 2024. [2](#), [8](#)
- [11] Yiqun Duan, Xianda Guo, and Zheng Zhu. Diffusiondepth: Diffusion denoising approach for monocular depth estimation. arXiv preprint arXiv:2303.05021, 2023. [1](#), [3](#), [4](#)
- [12] Ainaz Eftekhari, Alexander Sax, Jitendra Malik, and Amir Zamir. Omnidata: A scalable pipeline for making multi-task mid-level vision datasets from 3d scans. In Proceedings of the IEEE/CVF International Conference on Computer Vision, pages 10786–10796, 2021. [3](#), [6](#)
- [13] David Eigen and Rob Fergus. Predicting depth, surface normals and semantic labels with a common multi-scale convolutional architecture. In Proceedings of the IEEE international conference on computer vision, pages 2650–2658, 2015. [6](#), [1](#)
- [14] David Eigen, Christian Puhrsch, and Rob Fergus. Depth map prediction from a single image using a multi-scale deep network. Advances in neural information processing systems, 27, 2014. [6](#), [1](#)
- [15] Xiaohan Fei, Alex Wong, and Stefano Soatto. Geosupervised visual depth prediction. IEEE Robotics and Automation Letters, 4(2):1661–1668, 2019. [1](#)
- [16] Huan Fu, Mingming Gong, Chaohui Wang, Kayhan Batmanghelich, and Dacheng Tao. Deep ordinal regression network for monocular depth estimation. In Proceedings of the IEEE conference on computer vision and pattern recognition, pages 2002–2011, 2018. [2](#)
- [17] Xiao Fu, Wei Yin, Mu Hu, Kaixuan Wang, Yuexin Ma, Ping Tan, Shaojie Shen, Dahua Lin, and Xiaoxiao Long. Geowizard: Unleashing the diffusion priors for 3d geometry estimation from a single image. In European Conference on Computer Vision, pages 241–258. Springer, 2024. [1](#), [3](#), [6](#)
- [18] Adrien Gaidon, Qiao Wang, Johann Cabon, and Eleonora Vig. Virtual worlds as proxy for multi-object tracking analysis. In Proceedings of the IEEE conference on Computer Vision and Pattern Recognition, pages 4340–4349, 2016. [6](#), [1](#)
- [19] Peng Gao, Shijie Geng, Renrui Zhang, Teli Ma, Rongyao Fang, Yongfeng Zhang, Hongsheng Li, and Yu Qiao. Clip-adapter: Better vision-language models with feature adapters. arXiv preprint arXiv:2110.04544, 2021. [4](#)
- [20] Sicheng Gao, Xuhui Liu, Bohan Zeng, Sheng Xu, Yanjing Li, Xiaoyan Luo, Jianzhuang Liu, Xiantong Zhen, and Baochang Zhang. Implicit diffusion models for continuous super-resolution. In Proceedings of the IEEE/CVF conference on computer vision and pattern recognition, pages 10021–10030, 2023. [3](#)
- [21] Gonzalo Martin Garcia, Karim Abou Zeid, Christian Schmidt, Daan de Geus, Alexander Hermans, and Bastian Leibe. Fine-tuning image-conditional diffusion models is easier than you think. arXiv preprint arXiv:2409.11355, 2024. [1](#), [3](#)
- [22] Andreas Geiger, Philip Lenz, and Raquel Urtasun. Are we ready for autonomous driving? the kitti vision benchmark suite. In 2012 IEEE conference on computer vision and pattern recognition, pages 3354–3361. IEEE, 2012. [2](#), [6](#), [7](#), [1](#)
- [23] Andreas Geiger, Philip Lenz, Christoph Stiller, and Raquel Urtasun. Vision meets robotics: The kitti dataset. The International Journal of Robotics Research, 32(11):1231–1237, 2013. [6](#), [1](#), [2](#)
- [24] Ming Gui, Johannes Schusterbauer, Ulrich Prestel, Pingchuan Ma, Dmytro Kotovenko, Olga Grebenkova, Stefan Andreas Baumann, Vincent Tao Hu, and Björn Ommer. Depthfm: Fast monocular depth estimation with flow matching, 2024. [1](#), [3](#)
- [25] Jing He, Haodong Li, Wei Yin, Yixun Liang, Leheng Li, Kaiqiang Zhou, Hongbo Zhang, Bingbing Liu, and Yingcong Chen. Lotus: Diffusion-based visual foundation model for high-quality dense prediction. arXiv preprint arXiv:2409.18124, 2024. [1](#), [3](#)
- [26] Jonathan Ho, Ajay Jain, and Pieter Abbeel. Denoising diffusion probabilistic models. Advances in neural information processing systems, 33:6840–6851, 2020. [3](#), [4](#), [7](#), [2](#)

- [27] Jia Cheng Hu, Roberto Cavicchioli, and Alessandro Capotondi. Expansionnet v2: Block static expansion in fast end to end training for image captioning. [arXiv preprint arXiv:2208.06551](#), 2022. 8
- [28] Xueting Hu, Ce Zhang, Yi Zhang, Bowen Hai, Ke Yu, and Zhihai He. Learning to adapt clip for few-shot monocular depth estimation. [arXiv preprint arXiv:2311.01034](#), 2023. 4
- [29] Yuanfeng Ji, Zhe Chen, Enze Xie, Lanqing Hong, Xihui Liu, Zhaoqiang Liu, Tong Lu, Zhenguo Li, and Ping Luo. Ddp: Diffusion model for dense visual prediction. In [Proceedings of the IEEE/CVF International Conference on Computer Vision](#), pages 21741–21752, 2023. 1, 3, 4
- [30] Bingxin Ke, Anton Obukhov, Shengyu Huang, Nando Metzger, Rodrigo Caye Daudt, and Konrad Schindler. Repurposing diffusion-based image generators for monocular depth estimation. [arXiv preprint arXiv:2312.02145](#), 2023. 1, 3, 4, 6, 7, 2
- [31] Moo Jin Kim, Karl Pertsch, Siddharth Karamcheti, Ted Xiao, Ashwin Balakrishna, Suraj Nair, Rafael Rafailov, Ethan Foster, Grace Lam, Pannag Sanketi, et al. Openvla: An open-source vision-language-action model. [arXiv preprint arXiv:2406.09246](#), 2024. 3
- [32] Dong Lao, Yangchao Wu, Tian Yu Liu, Alex Wong, and Stefano Soatto. Sub-token vit embedding via stochastic resonance transformers. In [International Conference on Machine Learning](#). PMLR, 2024. 2
- [33] Feng Li, Hao Zhang, Huaizhe Xu, Shilong Liu, Lei Zhang, Lionel M Ni, and Heung-Yeung Shum. Mask dino: Towards a unified transformer-based framework for object detection and segmentation. In [Proceedings of the IEEE/CVF Conference on Computer Vision and Pattern Recognition](#), pages 3041–3050, 2023. 8
- [34] Gang Li, Heliang Zheng, Chaoyue Wang, Chang Li, Changwen Zheng, and Dacheng Tao. 3ddesigner: Towards photorealistic 3d object generation and editing with text-guided diffusion models. [arXiv preprint arXiv:2211.14108](#), 2022. 3
- [35] Haoying Li, Yifan Yang, Meng Chang, Shiqi Chen, Huajun Feng, Zhihai Xu, Qi Li, and Yueting Chen. Srdiff: Single image super-resolution with diffusion probabilistic models. [Neurocomputing](#), 479:47–59, 2022. 3
- [36] Junnan Li, Dongxu Li, Caiming Xiong, and Steven Hoi. Blip: Bootstrapping language-image pre-training for unified vision-language understanding and generation. In [International Conference on Machine Learning](#), pages 12888–12900. PMLR, 2022. 3
- [37] Junnan Li, Dongxu Li, Silvio Savarese, and Steven Hoi. Blip-2: Bootstrapping language-image pre-training with frozen image encoders and large language models. [arXiv preprint arXiv:2301.12597](#), 2023. 3
- [38] Zhengqi Li and Noah Snavely. Megadepth: Learning single-view depth prediction from internet photos. In [Proceedings of the IEEE conference on computer vision and pattern recognition](#), pages 2041–2050, 2018. 3
- [39] Ce Liu, Suryansh Kumar, Shuhang Gu, Radu Timofte, and Luc Van Gool. Va-depthnet: A variational approach to single image depth prediction. [arXiv preprint arXiv:2302.06556](#), 2023. 2
- [40] Haotian Liu, Chunyuan Li, Yuheng Li, and Yong Jae Lee. Improved baselines with visual instruction tuning, 2023. 7, 3, 6
- [41] Minghua Liu, Ruoxi Shi, Linghao Chen, Zhuoyang Zhang, Chao Xu, Xinyue Wei, Hansheng Chen, Chong Zeng, Jiayuan Gu, and Hao Su. One-2-3-45++: Fast single image to 3d objects with consistent multi-view generation and 3d diffusion. In [Proceedings of the IEEE/CVF Conference on Computer Vision and Pattern Recognition](#), pages 10072–10083, 2024. 3
- [42] Andreas Lugmayr, Martin Danelljan, Andres Romero, Fisher Yu, Radu Timofte, and Luc Van Gool. Repaint: Inpainting using denoising diffusion probabilistic models. In [Proceedings of the IEEE/CVF conference on computer vision and pattern recognition](#), pages 11461–11471, 2022. 3
- [43] Jingcheng Ni, Weiguang Zhao, Daniel Wang, Ziyao Zeng, Chenyu You, Alex Wong, and Kaizhu Huang. Efficient interactive 3d multi-object removal. [arXiv preprint arXiv:2501.17636](#), 2025. 3
- [44] OpenAI. Chatgpt-4: Conversational ai model, 2024. Accessed via OpenAI’s platform for generating and refining content. 3
- [45] Maxime Oquab, Timothée Darcet, Théo Moutakanni, Huy Vo, Marc Szafraniec, Vasil Khalidov, Pierre Fernandez, Daniel Haziza, Francisco Massa, Alaaeldin El-Nouby, et al. Dinov2: Learning robust visual features without supervision. [arXiv preprint arXiv:2304.07193](#), 2023. 3
- [46] Guocheng Qian, Jinjie Mai, Abdullah Hamdi, Jian Ren, Aliaksandr Siarohin, Bing Li, Hsin-Ying Lee, Ivan Skokhodov, Peter Wonka, Sergey Tulyakov, et al. Magic123: One image to high-quality 3d object generation using both 2d and 3d diffusion priors. [arXiv preprint arXiv:2306.17843](#), 2023. 3
- [47] Longtian Qiu, Renrui Zhang, Ziyu Guo, Ziyao Zeng, Yafeng Li, and Guangnan Zhang. Vt-clip: Enhancing vision-language models with visual-guided texts. [arXiv preprint arXiv:2112.02399](#), 2021. 4
- [48] Alec Radford, Jong Wook Kim, Chris Hallacy, Aditya Ramesh, Gabriel Goh, Sandhini Agarwal, Girish Sastry, Amanda Askell, Pamela Mishkin, Jack Clark, et al. Learning transferable visual models from natural language supervision. In [International conference on machine learning](#), pages 8748–8763. PMLR, 2021. 3
- [49] Aditya Ramesh, Prafulla Dhariwal, Alex Nichol, Casey Chu, and Mark Chen. Hierarchical text-conditional image generation with clip latents. [arXiv preprint arXiv:2204.06125](#), 1(2):3, 2022. 3
- [50] René Ranftl, Katrin Lasinger, David Hafner, Konrad Schindler, and Vladlen Koltun. Towards robust monocular depth estimation: Mixing datasets for zero-shot cross-dataset transfer. [IEEE transactions on pattern analysis and machine intelligence](#), 44(3):1623–1637, 2020. 3, 6, 2
- [51] René Ranftl, Alexey Bochkovskiy, and Vladlen Koltun. Vision transformers for dense prediction. In [Proceedings of the IEEE/CVF international conference on computer vision](#), pages 12179–12188, 2021. 3, 6, 2

- [52] Yongming Rao, Wenliang Zhao, Guangyi Chen, Yansong Tang, Zheng Zhu, Guan Huang, Jie Zhou, and Jiwen Lu. Denseclip: Language-guided dense prediction with context-aware prompting. *arXiv preprint arXiv:2112.01518*, 2021. 4
- [53] Mike Roberts, Jason Ramapuram, Anurag Ranjan, Atulit Kumar, Miguel Angel Bautista, Nathan Paczan, Russ Webb, and Joshua M Susskind. Hypersim: A photorealistic synthetic dataset for holistic indoor scene understanding. In *Proceedings of the IEEE/CVF international conference on computer vision*, pages 10912–10922, 2021. 2, 6, 1
- [54] Robin Rombach, Andreas Blattmann, Dominik Lorenz, Patrick Esser, and Björn Ommer. High-resolution image synthesis with latent diffusion models. In *Proceedings of the IEEE/CVF conference on computer vision and pattern recognition*, pages 10684–10695, 2022. 3, 5, 7, 2
- [55] Chitwan Saharia, Jonathan Ho, William Chan, Tim Salimans, David J Fleet, and Mohammad Norouzi. Image super-resolution via iterative refinement. *IEEE transactions on pattern analysis and machine intelligence*, 45(4):4713–4726, 2022. 3
- [56] Tim Salimans and Jonathan Ho. Progressive distillation for fast sampling of diffusion models. *arXiv preprint arXiv:2202.00512*, 2022. 2
- [57] Saurabh Saxena, Abhishek Kar, Mohammad Norouzi, and David J Fleet. Monocular depth estimation using diffusion models. *arXiv preprint arXiv:2302.14816*, 2023. 1, 3, 4
- [58] Saurabh Saxena, Charles Herrmann, Junhwa Hur, Abhishek Kar, Mohammad Norouzi, Deqing Sun, and David J Fleet. The surprising effectiveness of diffusion models for optical flow and monocular depth estimation. *Advances in Neural Information Processing Systems*, 36, 2024. 1, 3, 4
- [59] Thomas Schops, Johannes L Schonberger, Silvano Galliani, Torsten Sattler, Konrad Schindler, Marc Pollefeys, and Andreas Geiger. A multi-view stereo benchmark with high-resolution images and multi-camera videos. In *Proceedings of the IEEE conference on computer vision and pattern recognition*, pages 3260–3269, 2017. 2, 6, 1
- [60] Nathan Silberman, Derek Hoiem, Pushmeet Kohli, and Rob Fergus. Indoor segmentation and support inference from rgbd images. In *Computer Vision—ECCV 2012: 12th European Conference on Computer Vision, Florence, Italy, October 7–13, 2012, Proceedings, Part V 12*, pages 746–760. Springer, 2012. 2, 6, 7, 1
- [61] Jiaming Song, Chenlin Meng, and Stefano Ermon. Denoising diffusion implicit models. *arXiv preprint arXiv:2010.02502*, 2020. 7, 2
- [62] Shengbang Tong, David Fan, Jiachen Zhu, Yunyang Xiong, Xinlei Chen, Koustuv Sinha, Michael Rabbat, Yann LeCun, Saining Xie, and Zhuang Liu. Metamorph: Multimodal understanding and generation via instruction tuning. *arXiv preprint arXiv:2412.14164*, 2024. 3
- [63] Ruoyu Wang, Yongqi Yang, Zhihao Qian, Ye Zhu, and Yu Wu. Diffusion in diffusion: Cyclic one-way diffusion for text-vision-conditioned generation. *arXiv preprint arXiv:2306.08247*, 2023. 3
- [64] Alex Wong, Safa Cicek, and Stefano Soatto. Targeted adversarial perturbations for monocular depth prediction. *Advances in neural information processing systems*, 33: 8486–8497, 2020. 2
- [65] Guangkai Xu, Yongtao Ge, Mingyu Liu, Chengxiang Fan, Kangyang Xie, Zhiyue Zhao, Hao Chen, and Chunhua Shen. What matters when repurposing diffusion models for general dense perception tasks? *arXiv preprint arXiv:2403.06090*, 2024. 1, 3
- [66] Fengyu Yang, Chao Feng, Ziyang Chen, Hyungseob Park, Daniel Wang, Yiming Dou, Ziyao Zeng, Xien Chen, Rit Gangopadhyay, Andrew Owens, and Alex Wong. Binding touch to everything: Learning unified multimodal tactile representations. In *Proceedings of the IEEE/CVF Conference on Computer Vision and Pattern Recognition*, 2024. 3
- [67] Fengyu Yang, Chao Feng, Daniel Wang, Tianye Wang, Ziyao Zeng, Zhiyang Xu, Hyungseob Park, Pengliang Ji, Hanbin Zhao, Yuanning Li, et al. Neurobind: Towards unified multimodal representations for neural signals. *arXiv preprint arXiv:2407.14020*, 2024. 3
- [68] Lihe Yang, Bingyi Kang, Zilong Huang, Xiaogang Xu, Jiashi Feng, and Hengshuang Zhao. Depth anything: Unleashing the power of large-scale unlabeled data. In *Proceedings of the IEEE/CVF Conference on Computer Vision and Pattern Recognition*, pages 10371–10381, 2024. 3, 6, 2
- [69] Lihe Yang, Bingyi Kang, Zilong Huang, Zhen Zhao, Xiaogang Xu, Jiashi Feng, and Hengshuang Zhao. Depth anything v2. *Advances in Neural Information Processing Systems*, 37:21875–21911, 2024. 3, 6
- [70] Shiyuan Yang, Xiaodong Chen, and Jing Liao. Uni-paint: A unified framework for multimodal image inpainting with pretrained diffusion model. In *Proceedings of the 31st ACM International Conference on Multimedia*, pages 3190–3199, 2023. 3
- [71] Wei Yin, Xinlong Wang, Chunhua Shen, Yifan Liu, Zhi Tian, Songcen Xu, Changming Sun, and Dou Renyin. Diversedepth: Affine-invariant depth prediction using diverse data. *arXiv preprint arXiv:2002.00569*, 2020. 3, 6
- [72] Wei Yin, Jianming Zhang, Oliver Wang, Simon Niklaus, Long Mai, Simon Chen, and Chunhua Shen. Learning to recover 3d scene shape from a single image. In *Proceedings of the IEEE/CVF Conference on Computer Vision and Pattern Recognition*, pages 204–213, 2021. 3, 6
- [73] Weihao Yuan, Xiaodong Gu, ZuoZhuo Dai, Siyu Zhu, and Ping Tan. Neural window fully-connected crfs for monocular depth estimation. In *Proceedings of the IEEE/CVF Conference on Computer Vision and Pattern Recognition*, pages 3916–3925, 2022. 2, 1
- [74] Ziyao Zeng, Daniel Wang, Fengyu Yang, Hyungseob Park, Stefano Soatto, Dong Lao, and Alex Wong. Worddepth: Variational language prior for monocular depth estimation. In *Proceedings of the IEEE/CVF Conference on Computer Vision and Pattern Recognition*, pages 9708–9719, 2024. 2, 3, 4
- [75] Ziyao Zeng, Yangchao Wu, Hyungseob Park, Daniel Wang, Fengyu Yang, Stefano Soatto, Dong Lao, Byung-Woo Hong, and Alex Wong. Rsa: Resolving scale ambiguities in monocular depth estimators through language descriptions. *arXiv preprint arXiv:2410.02924*, 2024. 3, 4, 6, 8, 1, 2

- [76] Chi Zhang, Wei Yin, Billzb Wang, Gang Yu, Bin Fu, and Chunhua Shen. Hierarchical normalization for robust monocular depth estimation. Advances in Neural Information Processing Systems, 35:14128–14139, 2022. 3, 6
- [77] Junbo Zhang, Runpei Dong, and Kaisheng Ma. Clip-fo3d: Learning free open-world 3d scene representations from 2d dense clip. In Proceedings of the IEEE/CVF International Conference on Computer Vision, pages 2048–2059, 2023. 4
- [78] Renrui Zhang, Rongyao Fang, Peng Gao, Wei Zhang, Kunchang Li, Jifeng Dai, Yu Qiao, and Hongsheng Li. Tip-adapter: Training-free clip-adapter for better vision-language modeling. arXiv preprint arXiv:2111.03930, 2021. 4
- [79] Renrui Zhang, Ziyao Zeng, Ziyu Guo, Xinben Gao, Kexue Fu, and Jianbo Shi. Dspoint: Dual-scale point cloud recognition with high-frequency fusion. arXiv preprint arXiv:2111.10332, 2021. 3
- [80] Renrui Zhang, Ziyu Guo, Wei Zhang, Kunchang Li, Xupeng Miao, Bin Cui, Yu Qiao, Peng Gao, and Hongsheng Li. Pointclip: Point cloud understanding by clip. In Proceedings of the IEEE/CVF Conference on Computer Vision and Pattern Recognition, pages 8552–8562, 2022. 4
- [81] Renrui Zhang, Ziyao Zeng, Ziyu Guo, and Yafeng Li. Can language understand depth? In Proceedings of the 30th ACM International Conference on Multimedia, pages 6868–6874, 2022. 2, 3, 4
- [82] Wenliang Zhao, Yongming Rao, Zuyan Liu, Benlin Liu, Jie Zhou, and Jiwen Lu. Unleashing text-to-image diffusion models for visual perception. arXiv preprint arXiv:2303.02153, 2023. 4
- [83] Wenliang Zhao, Yongming Rao, Zuyan Liu, Benlin Liu, Jie Zhou, and Jiwen Lu. Unleashing text-to-image diffusion models for visual perception. In Proceedings of the IEEE/CVF International Conference on Computer Vision, pages 5729–5739, 2023. 1, 3, 4
- [84] Chong Zhou, Chen Change Loy, and Bo Dai. Denseclip: Extract free dense labels from clip. arXiv preprint arXiv:2112.01071, 2021. 4
- [85] Junsheng Zhou, Jinsheng Wang, Baorui Ma, Yu-Shen Liu, Tiejun Huang, and Xinlong Wang. Uni3d: Exploring unified 3d representation at scale. arXiv preprint arXiv:2310.06773, 2023. 4
- [86] Kingyi Zhou, Rohit Girdhar, Armand Joulin, Philipp Krähenbühl, and Ishan Misra. Detecting twenty-thousand classes using image-level supervision. In European Conference on Computer Vision, pages 350–368. Springer, 2022. 4, 8
- [87] Xiangyang Zhu, Renrui Zhang, Bawei He, Ziyu Guo, Ziyao Zeng, Zipeng Qin, Shanghang Zhang, and Peng Gao. Pointclip v2: Prompting clip and gpt for powerful 3d open-world learning. In Proceedings of the IEEE/CVF International Conference on Computer Vision, pages 2639–2650, 2023. 3, 4
- [88] Ye Zhu, Yu Wu, Kyle Olszewski, Jian Ren, Sergey Tulyakov, and Yan Yan. Discrete contrastive diffusion for cross-modal music and image generation. arXiv preprint arXiv:2206.07771, 2022. 3
- [89] Ye Zhu, Yu Wu, Zhiwei Deng, Olga Russakovsky, and Yan Yan. Boundary guided learning-free semantic control with diffusion models. Advances in Neural Information Processing Systems, 36, 2024. 3

# PriorDiffusion: Leverage Language Prior in Diffusion Models for Monocular Depth Estimation

## Supplementary Material

### A. Dataset Details

We train our model on two synthetic datasets, Hypersim [53] and Virtual Kitti [3], and conduct zero-shot evaluations on four additional real-world datasets that were not part of its training data, NYUv2 [60], KITTI [22], ScanNet [9], and ETH3D [59]. Details of each dataset are provided below.

#### A.1. Training Datasets

**Hypersim** [53] is a photorealistic synthetic dataset designed for comprehensive indoor scene understanding, and is introduced since obtaining per-pixel ground truth labels from real images is often challenging or impossible for many essential scene understanding tasks. This dataset is created using a vast collection of synthetic scenes developed by professional artists, resulting in 77,400 images across 461 indoor scenes with detailed per-pixel annotations and corresponding ground truth geometry. HyperSim is built exclusively using publicly accessible 3D assets. It includes complete scene geometry, material properties, and lighting information for each scene. Also, it provides dense per-pixel semantic instance segmentations and comprehensive camera details for each image. Further, it decomposes each image into diffuse reflectance, diffuse illumination, and a non-diffuse residual component that captures view-dependent lighting effects. In terms of training split, as mentioned in the Experiments Section, we utilize the official dataset split to select approximately 54,000 samples from 365 scenes, ensuring that any incomplete samples are excluded. The RGB images and depth maps are resized to a resolution of  $480 \times 640$  pixels, and the original distance measurements, defined relative to the focal point, are transformed into standard depth values relative to the focal plane.

**Virtual Kitti** [3, 18] Virtual KITTI is a photorealistic synthetic video dataset created for training and evaluating computer vision models on various video understanding tasks, including object detection, multi-object tracking, scene-level and instance-level semantic segmentation, optical flow, and depth estimation. The dataset comprises 50 high-resolution monocular videos (a total of 21,260 frames) generated from five distinct virtual urban environments, each presented under varying imaging and weather conditions. These virtual scenes were developed using the Unity game engine and an innovative real-to-virtual cloning technique. The synthetic videos come with precise, fully automatic annotations for 2D and 3D multi-object tracking, as well as per-pixel category, instance, flow, and depth labels.

We use its upgraded version, Virtual KITTI 2 [3], which consists of the same five sequence clones as Virtual KITTI, with increased photorealism. It takes advantage of recent advancements in lighting and post-processing within the game engine, making the variations in the virtual sequences more closely mimic real-world changes in conditions. For training, we choose four scenes, comprising around 20,000 samples, and crop the images to match the resolution of the KITTI benchmark [22]. The maximum depth is capped at 80 meters.

#### A.2. Evaluation Datasets

**NYUv2** [60] dataset comprises 24,231 synchronized RGB images and depth maps at a resolution of  $640 \times 480$ , representing various indoor scenes such as homes, offices, and commercial spaces, captured using a Microsoft Kinect. The standard split includes 249 training scenes and 215 test scenes. For our experiments, we use the official test set. Consistent with prior works [2, 30, 73–75], we exclude samples without valid ground truth, resulting in 654 valid images for evaluation. We perform evaluation on NYUv2 over a depth range spanning from  $1 \times 10^{-3}$  to 10 meters.

**KITTI** [22, 23] contains 61 driving scenes with research in autonomous driving and computer vision. It contains calibrated RGB images with synchronized point clouds from Velodyne lidar, inertial, GPS information, etc. Following prior works [2, 30, 73–75], we used Eigen split [13]. It consists of 652 testing images after filtering out images without valid ground truth. We follow the evaluation protocol of [14] for our experiments.

**ScanNet** [9] is an extensive RGB-D video dataset containing 2.5 million views in more than 1500 scans, annotated with 3D camera poses, surface reconstructions, and instance-level semantic segmentations. Data was collected using an RGB-D capture system (with a Kinect sensor) that includes automated surface reconstruction and crowd-sourced semantic annotation. We use the same evaluation configuration of Marigold [30], where 800 images are randomly selected from the 312 official validation scenes for evaluation.

**ETH3D** [59] is a multi-view stereo and 3D reconstruction benchmark encompassing a diverse range of indoor and outdoor scenes. High-precision laser scanning was used to obtain the ground truth geometry. Images were captured using both a DSLR camera and a synchronized multi-camera rig with varying fields-of-view. For evaluation, following Marigold [30], we use all 454 samples that include ground

truth depth maps.

## B. Implementation Details

### B.1. Visualization

When visualizing the ground truth depth map, we apply the same affine transformation we used in training. As described in the Experiments Section, we apply a linear normalization ensuring that the depth values primarily fall within the range  $[-1, 1]$ . The affine transformation for normalization is defined as:

$$\tilde{y}^* = \left( \frac{y^* - y_2}{y_2 - y_{98}} - 0.5 \right) \times 2, \quad (2)$$

where  $y_2$  and  $y_{98}$  represent the 2% and 98% percentiles of the depth maps, respectively. Then, we apply min-max normalization to both the ground truth and predicted depth maps, scaling them to integer values within the range  $[0, 255]$ . These normalized depth maps are then visualized using the OpenCV MAGMA colormap.

It is important to note that, unlike Marigold [30], which applies linear fitting to the ground truth for error correction, we do not use this approach. While linear fitting can adjust predictions to more closely align with the ground truth, it does not accurately reflect the true distribution of the depth map predictions or provide a clear assessment of prediction quality. Instead, we enhance visualization by applying the same training normalization to the zero-shot evaluation dataset, avoiding linear fitting and its error correction effects, resulting in more authentic and insightful visualization outcomes.

### B.2. Training details.

We implemented our method using PyTorch, employing Stable Diffusion v2 [54] as the backbone and maintaining the original pre-training configuration with the  $v$ -objective [56]. The training process utilized the DDPM noise scheduler [26] with 1,000 diffusion steps, while at inference time, the DDIM scheduler [61] was employed with 50 sampling steps for faster results. Our training setup spanned 30,000 iterations, with an effective batch size of 32 achieved through gradient accumulation over 16 steps (with a per-step batch size of 2) to fit on a single Nvidia RTX 3090 GPU. We used the Adam optimizer with a learning rate set at  $3 \cdot 10^{-5}$  and included random horizontal flipping with a probability of 0.5 as data augmentation. For depth normalization, we employed a scale and shift-invariant method with clipping enabled and set the normalization range between -1.0 and 1.0, using a 0.02 min-max quantile to maintain robustness. This normalization strategy was applied during training and zero-shot evaluations for consistency. The training noise scheduler initialized from the pre-trained Stable Diffusion v2 [54] model maintained a noise strength

of 0.9 and incorporated an annealed strategy to progressively reduce noise levels. We saved checkpoints every 50 iterations, with backup, validation, and visualization checkpoints set at intervals of 2,000 iterations. The training process typically converged after approximately 20,000 iterations, though we extended training to 30,000 iterations for thorough coverage. We used mean squared error (MSE) as the loss function, with reduction set to “mean” for averaged loss calculation. A customized iteration-wise exponential scheduler is applied which adjusts the learning rate iteratively using an exponential decay function. It decays the learning rate to 1% of its initial value over 25,000 iterations with a warmup phase of 100 steps. For text generation, generating a single caption for an image using LLaVA v1.6 on an RTX 3090 takes approximately 3.6 seconds, and we generate 10 captions for each image. For training, we generate 740,000 captions, using 740 GPU hours on an RTX 3090.

### B.3. Evaluation metric

Following the affine-invariant depth evaluation protocol [30, 50, 51, 68, 75], for each image and the predicted relative depth  $y$ , we fit a pair of scalars denoting the scale and shift parameters of the transformation:  $(\hat{\alpha}, \hat{\beta}) = g_\psi(y, y^*) \in \mathbb{R}^2$ . The metric depth prediction is obtained by  $\hat{y} = \hat{\alpha} \cdot y + \hat{\beta}$  such that:

$$\psi^* = \arg \min_{\psi} \frac{1}{|M|} \sum_{(i,j) \in \Omega} M(i,j) |\hat{y}(i,j) - y(i,j)| \quad (3)$$

where  $\hat{y} = \hat{\alpha} \cdot y + \hat{\beta}$  denotes the predicted metric-scale depth aligned from relative depth  $y$ ,  $(i, j) \in \Omega$  denotes an image coordinate, and  $M : \Omega \mapsto \{0, 1\}$  denotes a binary mask indicating valid coordinates in the ground truth depth  $y^*$  with values greater than zero. Then, we follow [5, 39, 74, 75, 81] to evaluate using first-order threshold accuracy, calculated as:

$$\delta_1 = \% \text{ of } y(i, j) \text{ s.t. } \max\left(\frac{y(i, j)}{y^*(i, j)}, \frac{y^*(i, j)}{y(i, j)}\right) < 1.25 \quad (4)$$

and mean absolute relative error, calculated as:

$$AbsRel = \frac{1}{|M|} \sum_{(i,j) \in \Omega} \frac{|y^*(i, j) - y(i, j)|}{y^*(i, j)} \quad (5)$$

## C. Additional Experiments

### C.1. Additional visualizations

We provide additional visualization and analysis for indoor scenes in Figure 10 and outdoor scenes in Figure 11. We use several samples in the NYUv2 [60] and KITTI [22, 23] dataset across diverse types of scenes. We have provided examples in captions under each figure. These visualizations demonstrate that leveraging the language prior within the

text-to-image diffusion model enhances the model’s ability to understand the geometric characteristics of the specified regions and objects. It shows that language plays a critical role in guiding the model’s attention to relevant regions and providing context for improved depth prediction. It highlights subtle or easily overlooked details, such as small objects or instances, and enhances the perception of complex scenes with multiple objects or intricate surfaces. Additionally, language descriptions offer an essential context for partially observed or occluded objects, enabling the model to infer details that visual cues alone might miss. By integrating language prior, the model achieves a more comprehensive and accurate understanding of scenes, especially in challenging scenarios.

### C.2. Ablation for prompts to generate text

To study the effect of different prompts for text generation, here we use the visual question-answering model LLaVA v1.6 Mistral [40] to generate one text for each training image and testing image. The prompt we use should elicit responses that capture essential details, including the positioning of objects, their interactions, and notable features that influence monocular depth estimation. We generate different prompts using ChatGPT 4o [44], with the prompt:

*“Generate prompt for a vision-language model to generate language description for each given image in one sentence. The prompt we use needs to elicit responses that include essential details, such as the positioning of objects, their interactions, and notable features that may impact depth estimation.”*

We present the results in Table 3, showcasing various language descriptions generated by LLaVA under different prompts. While the performances exhibit some variation, they remain consistently comparable. This demonstrates that as long as meaningful language descriptions of 3D scenes, resembling natural descriptions provided by humans, are provided, PriorDiffusion can effectively leverage the language prior to enhance monocular depth estimation.

### C.3. Different denoising steps.

As demonstrated in Figure 8, we evaluate PriorDiffusion and Marigold with different denoising steps during inference. The extracted performances are shown in Table 4. With more denoising steps, performance gradually improves. PriorDiffusion consistently outperforms Marigold across various denoising steps, converging in just 10 steps, while Marigold requires 25 steps. This suggests that the language prior could offer a good initialization, speeding up the denoising process and accelerating convergence.

### C.4. Template prompt comparison.

In situations where user-provided descriptions are not available, we aim to explore whether our method can still per-

Method	NYUv2		KITTI		ETH3D	
	$\delta_1 \uparrow$	AbsRel $\downarrow$	$\delta_1 \uparrow$	AbsRel $\downarrow$	$\delta_1 \uparrow$	AbsRel $\downarrow$
“An image”	95.7	6.1	89.8	10.7	95.1	6.8
Template A	95.8	6.0	90.3	10.6	95.5	6.4
Template B	95.7	6.1	90.5	10.7	95.6	6.5
Template C	<b>95.9</b>	6.0	90.2	10.6	95.3	6.6
Template D	95.6	<b>5.8</b>	90.4	10.5	95.4	6.4
Template E	95.8	5.9	90.3	10.7	95.6	6.7
Template F	<b>95.9</b>	6.0	90.5	10.5	95.4	6.6
Template G	95.8	6.1	90.3	10.6	95.5	<b>6.3</b>
Template H	95.7	5.9	90.2	10.7	<b>95.7</b>	<b>6.3</b>
Template I	95.8	6.1	<b>90.6</b>	10.5	95.4	6.6
Template J	95.8	6.0	90.5	10.6	95.6	6.4
Template K	95.7	<b>5.8</b>	90.4	10.5	95.5	<b>6.3</b>
Ours	<b>95.9</b>	5.9	<b>90.6</b>	<b>10.4</b>	<b>95.7</b>	6.5

Template A: “Describe the image in one sentence. Explain the image by identifying key objects and their distances from the viewpoint, noting any perspective lines or depth cues that indicate the three-dimensional structure of the scene.”

Template B: “Describe the image in one sentence. Describe the image by detailing the foreground, midground, and background objects, emphasizing their relative distances and spatial positioning within the scene.”

Template C: “Describe the image in one sentence. Describe the image by detailing the foreground, midground, and background objects, emphasizing their relative distances and spatial positioning within the scene.”

Template D: “Describe the image in one sentence. Provide an in-depth description of the image, focusing on the scale and depth of each visible object and how they overlap or are spaced from one another.”

Template E: “Describe the image in one sentence. Analyze the image by discussing the size and arrangement of objects, their positions relative to one another, and any changes in texture or clarity that indicate varying depths across the scene.”

Template F: “Describe the image in one sentence. Describe the scene with attention to depth, specifying which elements appear closer or farther from the viewer and how shadows or lighting contribute to the perception of depth.”

Template G: “Describe the image in one sentence. Highlight the depth relationships in the image by describing which objects are in the foreground, which are in the background, and how their relative sizes help convey distance.”

Template H: “Describe the image in one sentence. Focus on any natural or man-made structures in the image and describe how their orientation and placement give a sense of depth or perspective.”

Template I: “Describe the image in one sentence. Describe how elements like roads, pathways, or fences create leading lines that guide the viewer’s eye into the depth of the scene.”

Template J: “Describe the image in one sentence. Explain how differences in lighting or shadowing in the image indicate which parts are nearer or further away from the observer.”

Template K: “Describe the image in one sentence. Analyze the spatial arrangement of the main objects and describe any overlapping or occlusion that suggests depth relationships between them.”

Ours: “Describe the image in one sentence, assuming it’s a real-world image, pay more attention to objects, their spatial relationships, and the overall layout.”

Table 3. **Ablation for prompts to generate language description.** Prompts are used to prompt LLaVA to generate language descriptions for each image. While the performances among different prompts may vary, they remain consistently comparable, as long as they are meaningful and mimic human descriptions.

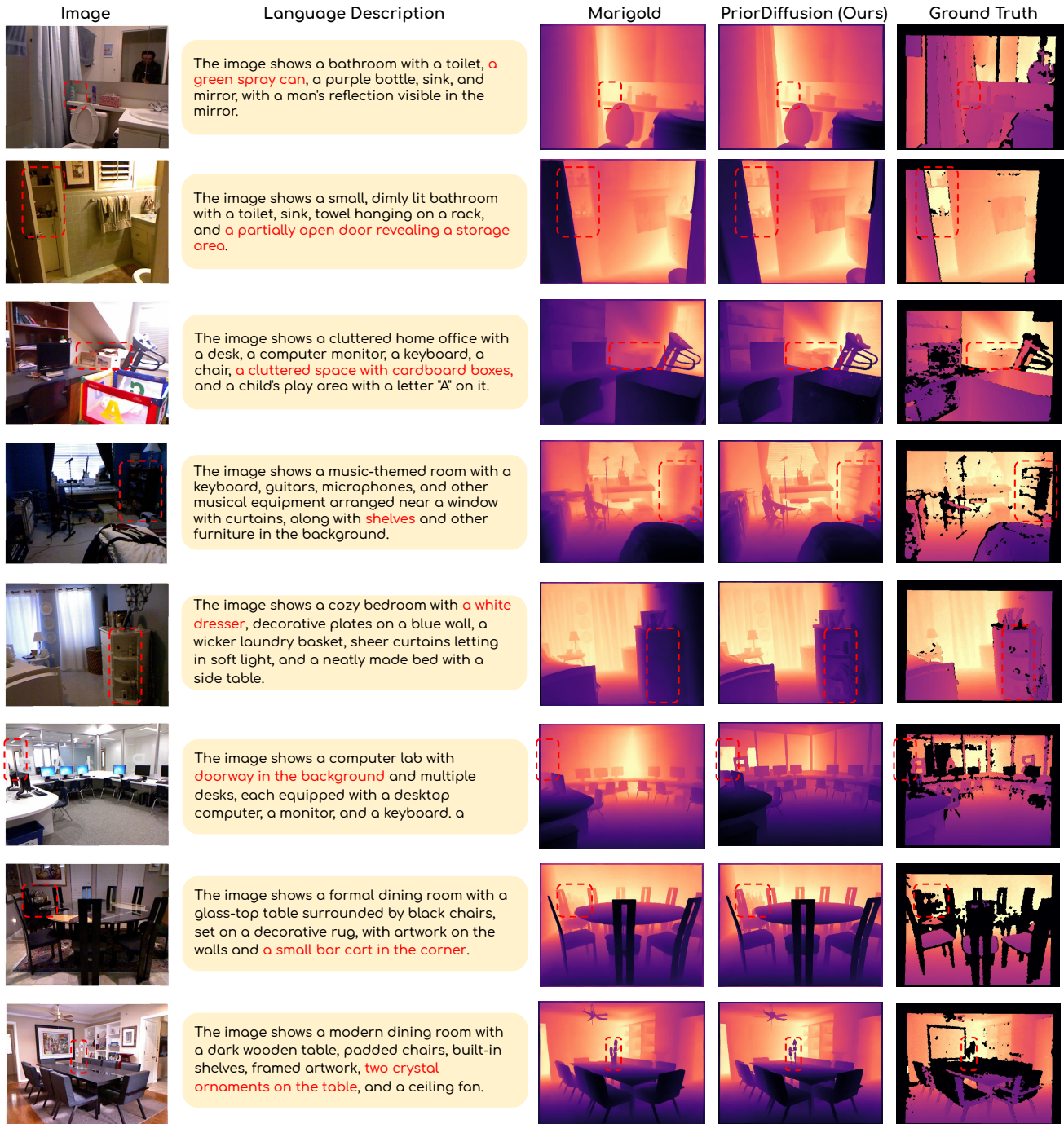


Figure 10. **Additional visualization on NYUv2.** Compared to Marigold, our PriorDiffusion demonstrates better depth prediction, particularly for instances specified in the language description (highlighted in red text and marked with red boxes). The language description effectively guides the model’s attention to relevant regions, especially those easily overlooked by visual cues due to a small size or a transparent texture, such as “a green spray can” in the 1st row and “two crystal ornaments” in the last row. It also improves perception under challenging visual conditions, like “shelves” in the 4th row and “a white dresser” in the 5th row, both of which are under poor illumination and are difficult to tell from visual solely. Additionally, it supports complex reasoning about scene layouts that might be misinterpreted from visual cues alone, such as “a doorway in the background” in the 6th row. Furthermore, it provides critical context for partially observed or occluded objects, such as “a partially open door revealing a storage area” in the 2nd row and “a small bar cart in the corner” in the 7th row.

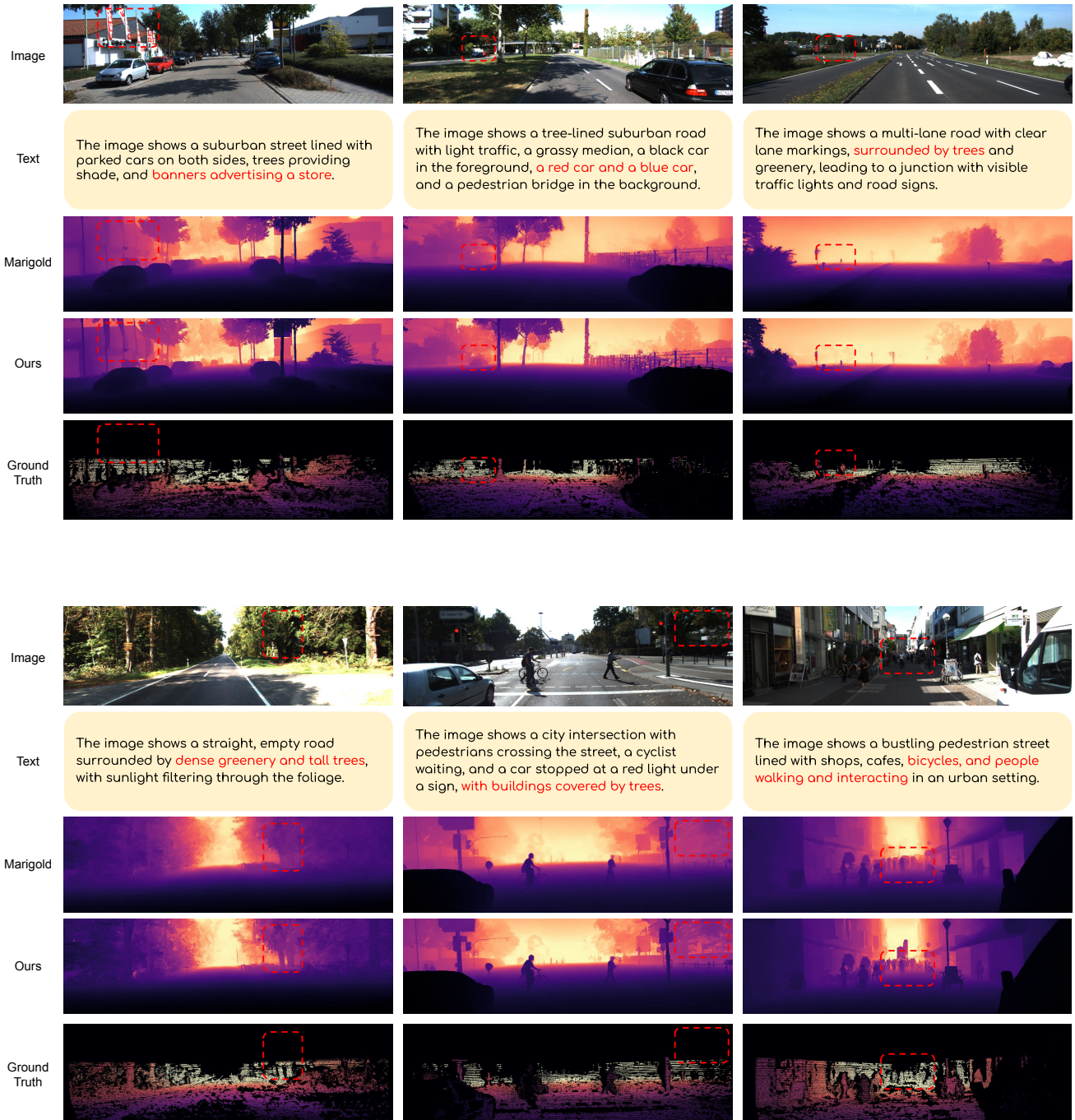


Figure 11. **Additional visualization on KITTI.** Compared to Marigold, our PriorDiffusion demonstrates superior depth prediction, particularly for instances specified in the language description (highlighted in red text and marked with red boxes). The language description effectively guides the model’s attention to relevant regions that might otherwise be overlooked due to their small size or subtle visual cues. Examples include “banners advertising a store” in the upper 1st column and “a red car and a blue car” in the upper 2nd column. Additionally, it enhances perception in complex scenes featuring multiple objects or intricate surfaces. For instance, it accurately captures “surrounded by trees” in the lower 1st column, “dense greenery and tall trees” in the upper 3rd column, and “bicycles, and people walking and interacting” in the lower 3rd column. Furthermore, the language descriptions provide essential context for partially observed or occluded objects, such as “buildings covered by trees” in the lower 2nd column.

Steps	NYUv2		KITTI		ETH3D		ScanNet	
	$\delta_1 \uparrow$	AbsRel $\downarrow$						
<b>Marigold</b>								
1	48.8	33.8	25.2	59.1	50.1	37.5	60.3	25.7
2	78.7	16.9	72.2	18.0	86.0	12.7	72.1	19.2
3	92.6	8.2	77.7	15.3	92.0	8.6	87.1	11.4
4	94.2	7.0	80.4	14.1	93.6	7.6	90.7	9.3
5	94.7	6.7	82.4	13.4	94.3	7.3	91.9	8.6
10	95.1	6.4	86.5	11.9	94.9	6.9	93.2	7.8
15	95.1	6.4	87.4	11.6	95.0	6.9	93.4	7.7
20	95.2	6.3	88.0	11.4	95.0	6.9	93.7	7.5
25	95.3	6.3	88.2	11.3	95.0	6.9	93.7	7.5
50	95.3	6.3	88.5	11.2	95.0	6.9	93.8	7.5
<b>PriorDiffusion</b>								
1	48.8	33.8	25.2	59.1	50.1	37.5	60.3	25.7
2	83.2	14.1	74.7	16.9	86.5	12.0	75.0	17.8
3	94.3	7.1	81.2	13.9	93.0	7.7	90.6	9.5
4	95.5	6.3	84.7	12.4	94.7	6.9	93.5	7.8
5	95.7	6.0	87.0	11.6	95.3	6.6	91.9	8.6
10	96.0	5.9	89.9	10.5	95.7	6.5	94.9	6.8
15	96.0	5.9	90.1	10.4	95.8	6.5	94.9	6.8
20	96.0	5.9	90.3	10.4	95.8	6.5	94.9	6.7
25	96.0	5.9	90.3	10.4	95.8	6.5	94.9	6.7
50	96.0	5.9	90.3	10.4	95.8	6.5	94.9	6.7

Table 4. **Performance for different denoising steps.** PriorDiffusion consistently outperforms Marigold across various denoising steps, with a significantly faster convergence speed for the diffusion process.

form effectively using either a blank input or standardized template prompts. If no specific language description that aligns with the scene is given by the user, we could instead use some pre-defined template prompt, such as “An image” or more elaborate prompts like, “A complex 3D scene with varying objects at different distances.”, as input of PriorDiffusion to maintain its performance. These templates, as presented in Table 5, assist in preserving the model’s performance when language input is not practical. Consequently, using template prompts as input during inference may differ from the training domain, leading to a significant covariate shift in language descriptions. This issue can be mitigated by incorporating template prompts as part of the input during training, enabling PriorDiffusion to better adapt to various scenarios where meaningful language descriptions are not feasible. Nevertheless, PriorDiffusion can achieve comparable or even better performance with Marigold when language input is not feasible, thus using a fixed prompt instead, showing that simply training with language can improve the performance of the depth estimator.

### C.5. Obtain language description.

To generate text descriptions for images, for training images, we use two different version of LLaVA v1.6 [40], Mistral and Vicuna, each with 5 different prompts, to generate 10 text descriptions for each training image:

- “Describe the image in one sentence, assuming it’s a real-world image.”
- “Provide a one-sentence description of the image, pay attention to object type, assuming it’s a real-world image.”

Method	NYUv2		KITTI		ETH3D	
	$\delta_1 \uparrow$	AbsRel $\downarrow$	$\delta_1 \uparrow$	AbsRel $\downarrow$	$\delta_1 \uparrow$	AbsRel $\downarrow$
Blank text input	95.5	6.2	89.3	10.9	95.0	6.9
“An image”	95.7	6.1	89.8	10.7	95.1	6.8
Template A	<b>95.8</b>	<b>6.0</b>	<b>89.9</b>	10.7	95.3	6.8
Template B	95.7	6.1	89.8	10.7	95.2	6.8
Template C	<b>95.8</b>	6.1	89.8	10.7	<b>95.3</b>	<b>6.8</b>
Marigold*	95.7	6.1	89.7	10.7	<b>95.4</b>	6.9
With text input	96.0	5.9	90.3	10.4	95.8	6.5

Template A: ‘A complex 3D scene with varying objects at different distances.’  
 Template B: ‘A structured environment with intricate patterns and designs that create depth and guide the eye through various focal points.’  
 Template C: ‘An elaborate scene with overlapping objects that create a sense of distance and spatial hierarchy within the environment.’

Table 5. **Template prompt comparison.** Metrics are reported as percentages. PriorDiffusion can achieve comparable or even better performance with Marigold when language input is not feasible, thus using a fixed prompt instead. The last row is the original PriorDiffusion with text input.

- “Capture the essence of the image in a single sentence, pay attention to object relationship, assuming it’s a real-world image.”
- “Condense the image description into one sentence, pay attention to object size, assuming it’s a real-world image.”
- “Express the image in just one sentence, pay attention to the overall layout, assuming it’s a real-world image.”

For testing images, we use LLaVA v1.6 Mistral, then prompt this model with:

- “Describe the image in one sentence, assuming it’s a real-world image. Pay close attention to objects, their spatial relationships, and the overall layout.”

This prompt is designed to elicit responses that include essential details, such as the positioning of objects, their interactions, and notable features that may impact depth estimation. Note that all training data we use are synthetic data, and by emphasizing “assuming it’s a real-world image,” we ensure that the descriptions align with the types of inputs and scenarios the model will encounter.